

Coupled magnetic and ferroelectric states in the distorted honeycomb system $\text{Fe}_4\text{Ta}_2\text{O}_9$


Soumendra Nath Panja,¹ Luminita Harnagea,¹ Jitender Kumar,¹ P. K. Mukharjee,² R. Nath,² A. K. Nigam,³ and Sunil Nair^{1,4}

¹*Department of Physics, Indian Institute of Science Education and Research, Dr. Homi Bhabha Road, Pune, Maharashtra 411008, India*

²*School of Physics, Indian Institute of Science Education and Research, Thiruvananthapuram 695016, India*

³*Department of Condensed Matter Physics and Material Science, Tata Institute of Fundamental Research, Dr. Homi Bhabha Road, Mumbai 400 005, India*

⁴*Centre for Energy Science, Indian Institute of Science Education and Research, Dr. Homi Bhabha Road, Pune, Maharashtra 411008, India*

 (Received 6 February 2018; revised manuscript received 30 April 2018; published 12 July 2018)

We report on the magnetic, thermodynamic, dielectric, and pyroelectric measurements on the hitherto unreported $\text{Fe}_4\text{Ta}_2\text{O}_9$. This system is seen to exhibit a series of magnetic transitions, many of which are coupled to the emergence of ferroelectric order, making $\text{Fe}_4\text{Ta}_2\text{O}_9$ the only genuine multiferroic in its material class. We suggest that the observed properties arise as a consequence of an effective reduction in the dimensionality of the magnetic lattice, with the magnetically active Fe^{2+} ions preferentially occupying a quasi-two-dimensional buckled honeycomb structure. The low-temperature H - T phase diagram of $\text{Fe}_4\text{Ta}_2\text{O}_9$ reveals a rich variety of coupled magnetic and ferroelectric phases similar to that observed in the distorted kagome systems.

DOI: [10.1103/PhysRevB.98.024410](https://doi.org/10.1103/PhysRevB.98.024410)

I. INTRODUCTION

Multiferroics, which refers to materials with concomitant magnetic and polar orders in a single system, continues to be at the forefront of contemporary condensed-matter physics [1]. Of particular interest are materials in which ferroelectric order arises as a direct consequence of nontrivial spin arrangements, and hence, the quest for new and improved multiferroics relies on identifying materials in which exotic spin structures (coupled with the antisymmetric Dzyaloshinskii-Moriya interaction) facilitate the breaking of spatial inversion symmetry [2–4]. Geometrically frustrated lattices provide a natural playground for exploring such exotic spin arrangements. This is especially true in low-dimensional systems, where a complex interplay between nearest and next-nearest exchange interactions, the single-ion anisotropy, and large spin-orbit coupling conspires to stabilize complex electronic and magnetic ground states. Examples include the $S = 1/2$ spin-chain system LiCu_2O_2 [5], the kagome-staircase compound $\text{Ni}_3\text{V}_2\text{O}_8$ [6], the buckled kagome system $\text{KCu}_3\text{As}_2\text{O}_7(\text{OD})_3$ [7], and the triangular lattice system CuFeO_2 [8], all of which exhibit novel coupling between the magnetic and polar order parameters.

The cross coupling between the magnetic and polar orders is a more generic phenomenon, the genesis of which can be traced to Dzyaloshinskii's pioneering work on Cr_2O_3 [9]. Here, a linear coupling between these order parameters arises as a direct consequence of the crystallographic symmetry, enabling one to manipulate the electric polarization (magnetization) by an applied magnetic (electric) field [10]. In this context, a family of tantalates and niobates of the form $A_4X_2O_9$ (where $A = \text{Mn}$ or Co and $X = \text{Ta}$ or Nb) has recently attracted extensive attention owing to its magnetoelectric properties. First synthesized by Bertaut *et al.* [11], this family of compounds crystallizes in the centrosymmetric trigonal $P\bar{3}c1$ space group, similar to the prototypical magnetoelectric Cr_2O_3 . The structure can be more accurately described as a variant of the corundum $\alpha\text{-Al}_2\text{O}_3$ with the A and X ions occupying

the Al sites in a ratio of 2:1. Within this structure, the A -site ions occupy two inequivalent crystallographic sites, and it has been suggested that both of them contribute independently to the magnetoelectric effect, with these contributions having opposite signs in the Co -based systems [12]. It is interesting to note that based on structural considerations alone, it was proposed that a member of this extended family, $\text{Mn}_4\text{Ta}_2\text{O}_9$, could harbor a ferroelectric ground state [13]. However, we note that these calculations relied on this system stabilizing in the $R\bar{3}c$ space group, which is at variance with experimental reports, where all members of the extended $A_4X_2O_9$ family are reported to be linear magnetoelectrics stabilizing in the trigonal $P\bar{3}c1$ symmetry [14–18].

Here, we report on $\text{Fe}_4\text{Ta}_2\text{O}_9$, a hitherto unexplored member of this family, using a combination of dc magnetization, specific-heat, dielectric, and pyroelectric measurements. Unlike all the other members of the $A_4X_2O_9$ family (which exhibit a solitary para-antiferromagnetic transition), this system exhibits a series of low-temperature magnetic transitions. Interestingly, many of these transitions are observed to be associated with the emergence of polar order, making $\text{Fe}_4\text{Ta}_2\text{O}_9$ the only known multiferroic in this material class. The low-temperature H - T phase diagram charted using our measurements shows some similarities with the kagome-staircase systems, making this a novel candidate to explore the intricate coupling between electrical polarization and nontrivial magnetic order.

II. EXPERIMENT

Polycrystalline samples of $\text{Fe}_4\text{Ta}_2\text{O}_9$ were prepared using an encapsulation synthesis technique, employing a sealed quartz ampoule which contained a homogeneous mixture of the precursors. Fe granules were used as an oxygen getter, allowing *in situ* control of the partial oxygen pressure. A stoichiometric ratio of previously preheated Fe_2O_3 and Ta_2O_5 was manually ground for a few hours in a glove box filled with argon, following which the mixture was transferred into

a ball-mill container and further ground under a static argon atmosphere. A preheated quartz ampoule ($\approx 25 \text{ cm}^3$) with two alumina crucibles was used for the sintering treatment. The larger alumina crucible was used to accommodate the oxygen getter (Fe grains, 1–2 mm), and the smaller one (filled with the mechanically homogenized mixture of precursors) was placed inside the larger crucible.

The ampoule charged in this fashion was evacuated, sealed under vacuum, and slowly heated to 1100°C and kept there for 48 h. The oxygen released during the reduction of Fe^{3+} to Fe^{2+} is continuously absorbed by the getter, thus stabilizing a pure $\text{Fe}_4\text{Ta}_2\text{O}_9$ end product, avoiding parasitic phases like FeTa_2O_6 , FeTaO_4 , and $\text{Fe}_3\text{Ta}_2\text{O}_8$. Phase purity of the compound was determined by room-temperature x-ray powder diffraction using Cu $K\alpha$ radiation. Low-temperature powder x-ray diffraction (XRD) measurements were carried out down to 15 K using a low- T attachment (Oxford Phenix) to the diffractometer (PANalytical). The powder XRD pattern was analyzed by the Rietveld method using the FULLPROF suite [19]. Elemental composition and homogeneity were further confirmed using an energy-dispersive x-ray spectrometer (Ziess Ultra Plus). Specific heat and dc magnetization were measured using a Quantum Design physical property measurement system and a MPMS-XL superconducting quantum interference device magnetometer, respectively. Dielectric measurements were performed using an Alpha-A high-performance frequency analyzer from Novocontrol Technologies. The pyroelectric measurements were performed in the parallel-plate geometry using a Keithley SourceMeter (model 2612B) and a picoammeter (model 6482). Zero-field pyroelectric measurements were performed in a closed-cycle refrigerator, and the magnetic-field-dependent dielectric and pyroelectric measurements were performed using the manual insertion utility probe of the MPMS-XL magnetometer. The polarization was deduced from the integration of measured pyroelectric current over time according to the formula $P = \int (I/A) dt$, where A is the area of the sample, I is the measured pyrocurrent, and t is the time.

III. RESULTS AND DISCUSSION

The Rietveld refinement of the room-temperature powder x-ray diffraction data is shown in Fig. 1(a). Like the other members of the $A_4\text{Ta}_2\text{O}_9$ family, this system is seen to crystallize in the centrosymmetric trigonal ($P\bar{3}c1$) symmetry. Along the crystallographic c axis, the structure of $\text{Fe}_4\text{Ta}_2\text{O}_9$ can be visualized to be made up of two distinct layers. The first layer (A) comprises hexagonal rings of edge-sharing Fe1O_6 octahedra, with the adjacent layer (B) being made up of alternating edge-sharing Fe2O_6 and TaO_6 octahedra, as schematically shown in Fig. 1(b) [20]. The structural details as obtained from the Rietveld refinement of room-temperature diffraction data are summarized in Table I. The chemical composition as obtained from the Rietveld analysis is found to be $\text{Fe}_{3.9\pm 0.1}\text{Ta}_{1.9\pm 0.1}\text{O}_9$. This is in agreement with the elemental composition determined using energy-dispersive x-ray analysis, which indicates a Fe:Ta ratio of $(3.93 \pm 0.12):(2.06 \pm 0.12)$.

The temperature dependence of dc magnetization as measured at 100 Oe in the zero-field-cooled (ZFC) and field-cooled (FC) protocols is shown in Fig. 2(a). On cooling from room

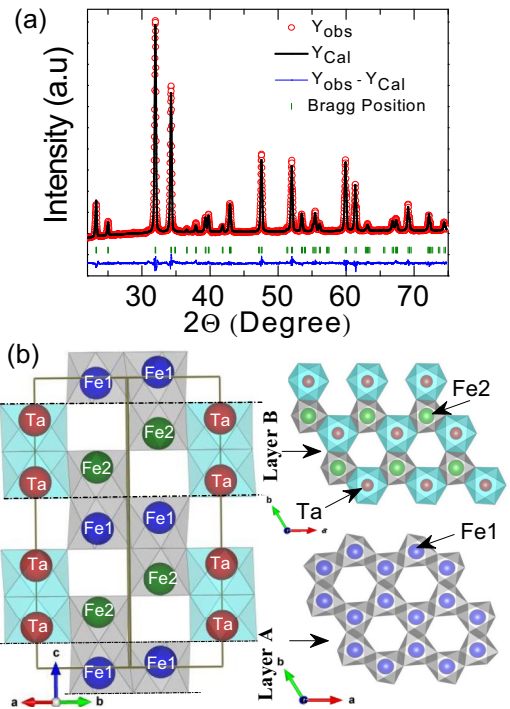


FIG. 1. (a) The Rietveld refinement of room-temperature x-ray diffraction data of $\text{Fe}_4\text{Ta}_2\text{O}_9$. This corresponds to a fit with R parameters of $R_{wp} = 9.13$, $R_e = 5.55$, and $\chi^2 = 2.7$. (b) The structure of this system, which can be viewed as a stack of alternating A and B layers along the crystallographic c axis.

temperature, two magnetic transitions at 80 K (T_1) and 60 K (T_2) are observed. These are more clearly evident from the temperature dependence of $d\chi/dt(T)$, as shown in the inset of Fig. 2(b). On further cooling, a splitting between the ZFC and FC curves is observed, with the magnetization increasing monotonically until a low-temperature magnetic transition T_3 at 5 K. The inverse of the dc magnetic susceptibility $\chi_{dc}^{-1}(T)$

TABLE I. Structural parameters of $\text{Fe}_4\text{Ta}_2\text{O}_9$ as determined from the Rietveld analysis of room-temperature x-ray diffraction data.

$\text{Fe}_4\text{Ta}_2\text{O}_9$				
Parameter	Value			
Temperature	296 K			
Space group	$P\bar{3}c1$ (No. 165)			
Crystal system	Trigonal			
a	5.232(4) Å			
b	5.232(4) Å			
c	14.238(1) Å			
$\alpha = \beta$	90°			
γ	120°			
Atom	Wyckoff	x/a	y/b	z/c
Fe1	4d	0.3333	0.6667	0.5172
Fe2	4d	0.3333	0.6667	0.3079
Ta	4c	0	0	0.8567
O1	6f	0.3112	0	0.2500
O2	12g	0.3288	0.2869	0.0817

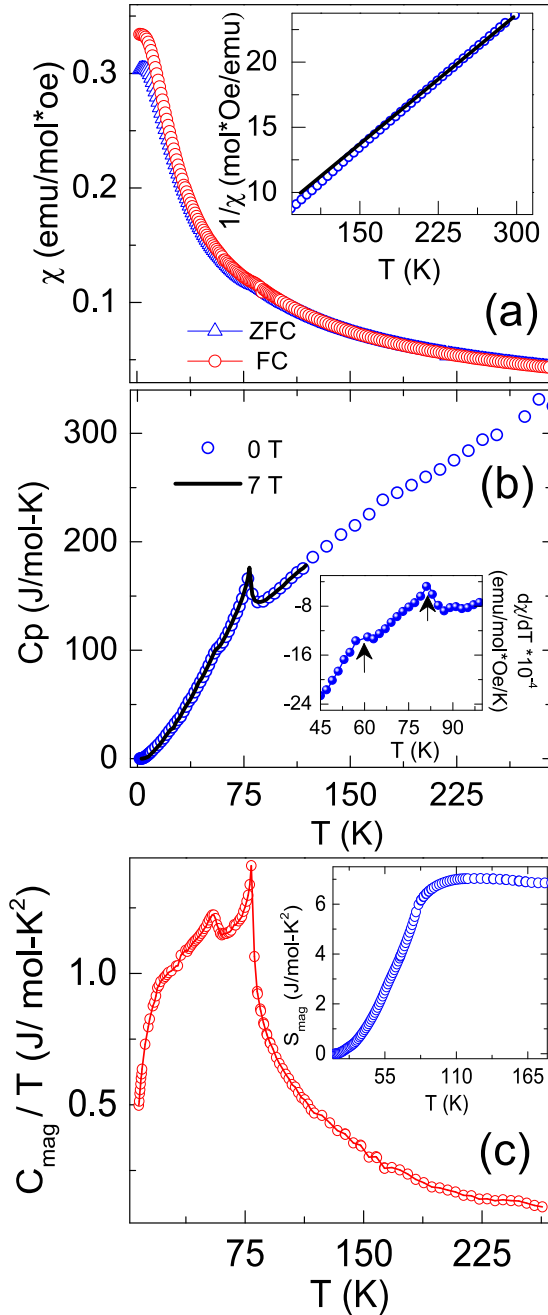


FIG. 2. (a) Temperature dependence of the dc magnetic susceptibility M/H as measured in ZFC and FC protocols at an applied magnetic field of 100 Oe. The inset shows a Curie-Weiss fit to the data in the high-temperature regime. (b) The inset depicts $d\chi/dT$ vs T , clearly indicating the presence of transitions at T_1 (80 K) and T_2 (60 K). The main panel depicts the temperature dependence of specific heat C_p as measured at 0 and 7 T. (c) The temperature dependence of the magnetic contribution to the specific heat C_{mag}/T . The inset shows the evolution of the magnetic entropy S_{mag} as a function of temperature.

is linear only above 150 K, as shown in the inset of Fig. 2(a), indicating the presence of short-range correlations well above the transition temperature. The linear fit to $\chi_{dc}^{-1}(T)$ gives a Curie-Weiss temperature θ_{CW} of -45.33 K, indicating mixed ferromagnetic and antiferromagnetic interactions. Sur-

prisingly, the calculated μ_B/Fe^{2+} as deduced from the Curie-Weiss fit is only $2.69\mu_B$, which is significantly less than the spin-only ($S = 2$) value of $4.89\mu_B$ expected from a Fe^{2+} ion in its high-spin state. This is also at variance with that observed in other members of the $A_4\text{Ta}_2\text{O}_9$ family, where the effective $\mu_B/\text{magnetic ion}$ is always seen to be larger than the corresponding spin-only value. This has been ascribed to indicate the presence of an unquenched orbital momentum contribution, which is also intimately related to the observed linear magnetoelectricity in those systems [12,18,21]. Our observations in $\text{Fe}_4\text{Ta}_2\text{O}_9$ indicate that Fe^{2+} coexists in both the high-spin ($S = 2$) and low-spin ($S = 0$) states in this system, and our Curie-Weiss fit indicates that the ratio of the high-spin:low-spin Fe^{2+} species is $\approx 0.55:0.45$. Specific-heat measurements reconfirm the presence of transitions at 80 and 60 K, as shown in Fig. 2(b), and measurements performed in the presence of a magnetic field also indicate that both of these anomalies are relatively insensitive to the application of magnetic fields up to 7 T. The magnetic contribution to specific heat C_{mag} calculated using the isostructural nonmagnetic $\text{Mg}_4\text{Ta}_2\text{O}_9$ indicates that 44% and 80% of the magnetic entropy S_{mag} are reached at the magnetic transitions at 60 and 80 K, respectively, and 20% of the entropy is released via short-range correlations above the transition. This is also in agreement with our observation that the Curie-Weiss behavior is valid only at temperatures well above the magnetic transition. The temperature dependence of the magnetic contribution to the specific heat C_{mag}/T and the magnetic entropy are depicted in the main panel and the inset of Fig. 2(c), respectively.

Dielectric measurements performed under zero magnetic field exhibit a weak anomaly at $T_1 = 80$ K and a pronounced feature at $T_2 = 60$ K [Fig. 3(a)]. Interestingly, pyrocurrent measurements also exhibit the appearance of features at both T_1 and T_2 , when the sample is poled from 85 K down to 35 K in the presence of different electric fields. This indicates that both these transitions could be accompanied by ferroelectric order. This is further confirmed by measurements in which the pyrocurrent was independently evaluated across *each* of these transitions, as shown in Fig. 3(b). This involved poling the sample from 70 K (i.e., $T_2 < T < T_1$), revealing a single peak in the pyrocurrent at 60 K, and subsequently poling the sample from 85 to 65 K, revealing a peak in the pyrocurrent at 80 K. Moreover, the sign of the pyrocurrent could be reversed in both cases by reversing the direction of the poling field, indicating the presence of two independent robust ferroelectric states at T_1 and T_2 . Our low-temperature x-ray diffraction measurement indicates that the crystallographic symmetry of $\text{Fe}_4\text{Ta}_2\text{O}_9$ remains invariant down to 15 K. Thus, the two anomalies observed in the magnetization and specific-heat measurements can be ascribed to magnetic ordering alone. The concomitant presence of magnetic and polar orders as evidenced by our magnetic and pyroelectric measurements indicates that $\text{Fe}_4\text{Ta}_2\text{O}_9$ is a genuine multiferroic. We note that this is in contrast to what is observed in other members of the $A_4\text{Ta}_2\text{O}_9$ family, all of which are reported to exhibit a solitary para-antiferromagnetic transition [16] and are reported to be linear magnetoelectrics, with polar order being observed only in the presence of an applied magnetic field.

Our low-temperature x-ray diffraction data also indicate that the onset of ferroelectric order is accompanied by an

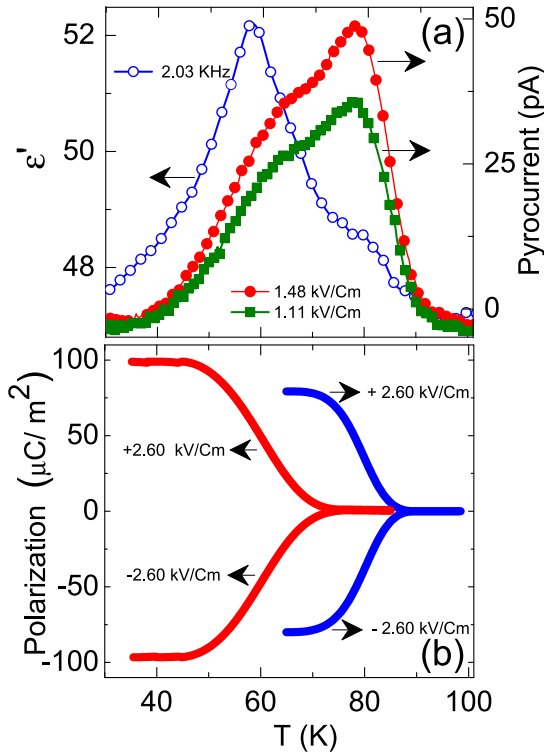


FIG. 3. (a) The dielectric constant ϵ' and the pyrocurrent in the vicinity of the transitions at T_1 (80 K) and T_2 (60 K). (b) The flipping of the polarization associated with these transitions on reversal of the poling electric field, indicating that they correspond to robust independent ferroelectric states.

abrupt change in the in-plane Fe1-O2 and the Fe2-O1 bond lengths, with the former decreasing (and the latter increasing) across this transition, as shown in Fig. 4(a). This represents a distortion of the polyhedral cage along the ab plane in the fashion shown in Fig. 4(b). Interestingly, this distortion does not appear to change the crystallographic structure in the sense that the diffraction patterns on either side of the phase transition could be fit using the same trigonal ($P\bar{3}c1$) symmetry. With no apparent change in the overall crystallographic symmetry within the resolution of our measurements, it is interesting to note that instead of exhibiting linear magnetoelectricity like the other members of the $A_4\text{Ta}_2\text{O}_9$ family, only this system appears to exhibit true polar order. We speculate that this could arise from an effective reduction in the dimensionality of the magnetic lattice in this system. Our magnetization data clearly indicate that approximately half of the Fe^{2+} ions in $\text{Fe}_4\text{Ta}_2\text{O}_9$ stabilize in the nonmagnetic ($S = 0$) state. In this context, it is interesting to note that the Fe^{2+} ions have two distinct crystallographic sites, Fe1 ($1/3, 1/3, 0.517$) and Fe2 ($1/3, 2/3, 0.307$), which lie in different planes stacked along the crystallographic c axis. As shown in Fig. 5, these two distinct lattice sites form separate distorted hexagonal sublattices along the ab plane, with the Fe1 sublattice being slightly buckled in nature [Fig. 5(a)] and the Fe2 sublattice having a zigzag like character [Fig. 5(b)]. If the different ($S = 2$ and $S = 0$) spin species of Fe^{2+} preferentially occupy the two possible crystallographic sites, we would expect to see this subtly reflected in the local octahedral environment of each

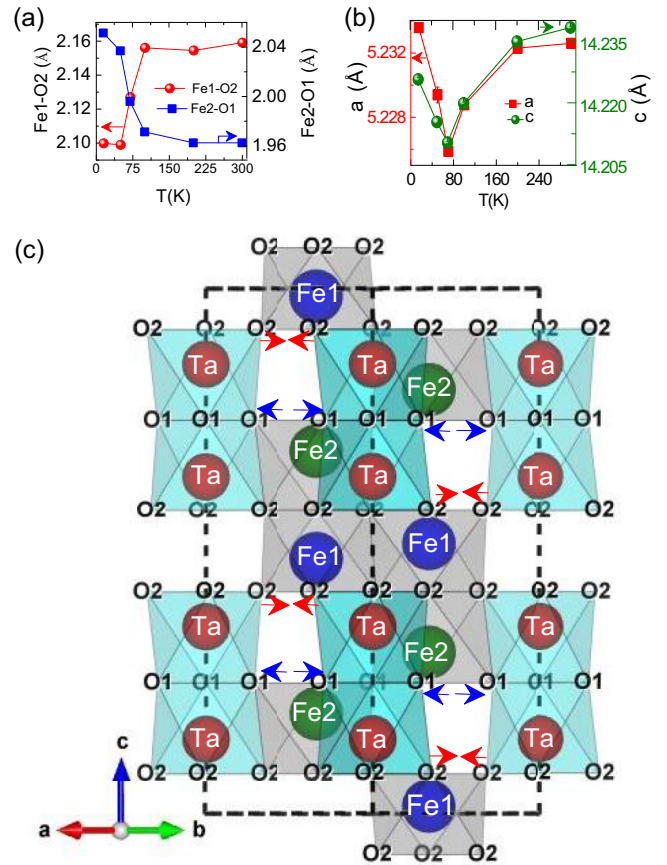


FIG. 4. (a) The variation of the Fe1-O and Fe2-O bond lengths across the magnetic transition. (b) The variation in the lattice parameters as a function of temperature. (c) The crystallographic structure of $\text{Fe}_4\text{Ta}_2\text{O}_9$ below the magnetic transition, where the buckling of the FeO polyhedra is observed.

of these FeO_6 subunits. Within an octahedral environment, a Fe^{2+} ($3d^6$) ion would be expected to have $t_{2g}^4 e_g^2$ and $t_{2g}^6 e_g^0$ electronic configurations in the high-spin and low-spin states, respectively. With the d orbitals of the occupied e_g electrons being along the direction of the oxygen $2p$ orbitals, the resultant Coulomb interaction would be expected to result in a slight elongation of the resultant bond, whereas the t_{2g} orbitals being directed along the bisector of the O-Fe-O angle would be expected to have a smaller effect. Analysis of our x-ray diffraction data indicates that the average Fe1-O bond length (2.16 Å) exceeds that of the Fe2-O bond length (2.05 Å) by 5%. For instance, in the case of the $[\text{Fe}(\text{phen})_2(\text{NCS})_2]$ molecule, with Fe^{2+} in an octahedral environment, it has been shown that the average Fe^{2+} -N bond length in the high-spin ($S = 2$) and low-spin ($S = 0$) states could differ by up to 9% [22]. We note that the low-spin state of Fe^{2+} is Jahn-Teller inactive within an octahedral environment and would thus not be a contributing factor. However, in its high-spin state, the t_{2g} orbitals of Fe^{2+} are Jahn-Teller active and could also possibly contribute to the observed octahedral distortion. This leads us to speculate that the magnetic ($S = 2$) Fe^{2+} ions exclusively occupy the buckled honeycomb sublattice, with the nonmagnetic ($S = 0$) Fe^{2+} ions occupying the alternating zigzag one. This basically reduces the dimensionality of the magnetic

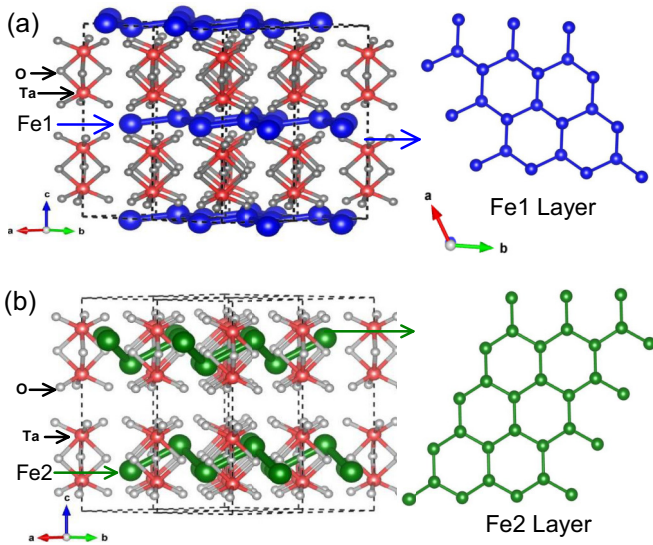


FIG. 5. (a) The buckled honeycomb lattice formed by the Fe1 ions separated by the nonmagnetic TaO₆ octahedra and (b) the zigzag chain of the nonmagnetic Fe2 ions. Considering the fact that the Fe1-O bond length is larger than the Fe2-O one, we speculate that the magnetic ($S = 2$) Fe²⁺ ions preferentially occupy the buckled honeycomb lattice and the nonmagnetic ($S = 0$) Fe²⁺ ions preferentially occupy the zigzag chain.

lattice from three-dimensional to quasi-two-dimensional. It is well known that short-range magnetic fluctuations can persist in a wide temperature window above the magnetic transition in two-dimensional magnets [23], signatures of which we have also observed in our magnetization measurements.

Measurements of the dc magnetic susceptibility measured in magnetic fields in excess of 1 T reveal the presence of an additional magnetic-field-induced transition. Appearing at ≈ 22 K at fields of the order of 1 T, the temperature at which this feature appears increases as a function of the applied magnetic field and reaches a maximum of ≈ 35 K at the highest applied magnetic field of 7 T, as is clearly evident from the $d(1/\chi)/dT$ vs T plot in Fig. 6(a). This field-induced transition is also clearly discernible in the dielectric measurements performed in the presence of magnetic fields in the form of a sharp downturn in the real part of the dielectric constant $\epsilon'(T, H)$, as seen in the inset of Fig. 6(b). This magnetic-field-induced transition was further evaluated by means of pyroelectric current measurements performed in the presence of different magnetic fields after typical magnetoelectric poling. This involved poling the specimen at different values of the electric (E) and magnetic (H) fields from a poling temperature of 50 K, with $E \perp H$. At low temperatures the electric field alone was removed, and standard pyroelectric measurements were performed in the presence of the magnetic field. As shown in the main panel of Fig. 6(b), this field-induced transition also manifests in the form of a sharp peak in the pyrocurrent. The polarization associated with this magnetic-field-induced transition can be fully flipped by reversing the direction of the electric and magnetic fields, as depicted in Fig. 6(c) for the case of measurements done at $H = 7$ T, indicating the true ferroelectric nature of this field-induced transition. The change in entropy associated with this magnetic-field-induced

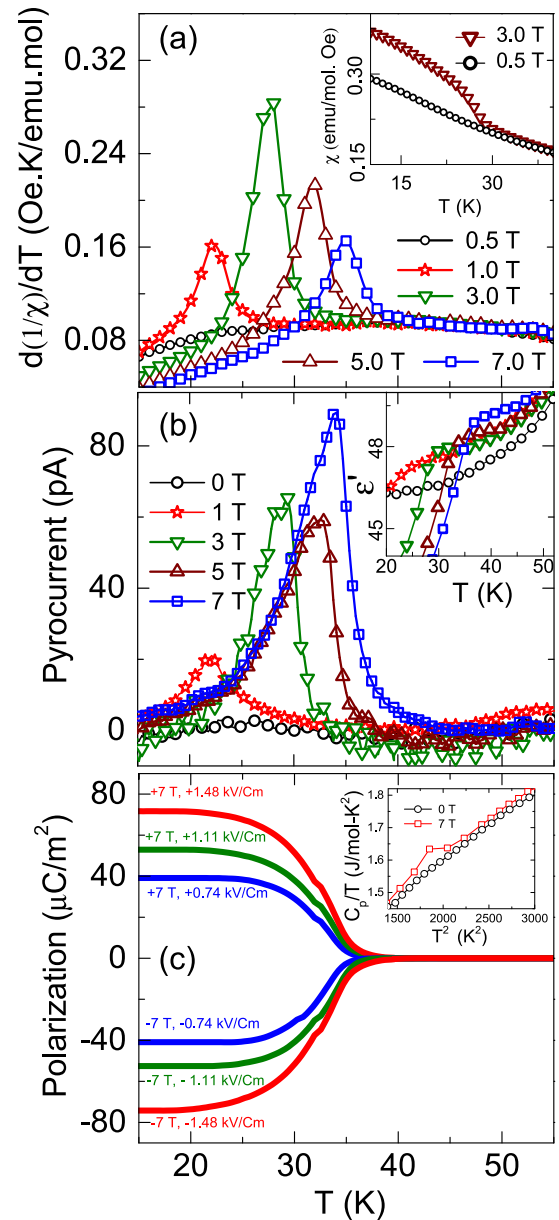


FIG. 6. (a) The inset depicts the dc magnetic susceptibility as measured at 5 kOe and 3 T, indicating the presence of a magnetic-field-induced transition. This is seen more clearly in the plots of the derivative $[d(1/\chi)/dt]$ vs T shown in the main panel. (b) The inset shows the temperature dependence of the dielectric constant ϵ' as measured at different magnetic fields, with sharp downturns being observed at the field-induced transition. This is also seen as a peak in the magnetic-field-dependent pyroelectric current measurements shown in the main panel. (c) Polarization obtained after integrating the pyrocurrent as measured in different electromagnetic poling conditions. A subtle signature corresponding to this magnetic-field-induced transition is also observed in the specific-heat data, as depicted in the inset.

transition is also reflected in the specific-heat data taken at $H = 7$ T, as depicted in the inset of Fig. 6(c).

Below this field-induced magnetic state, the ZFC magnetic susceptibility increases monotonically until the magnetic anomaly at 5 K [Fig. 7(a)]. Although this magnetic transition

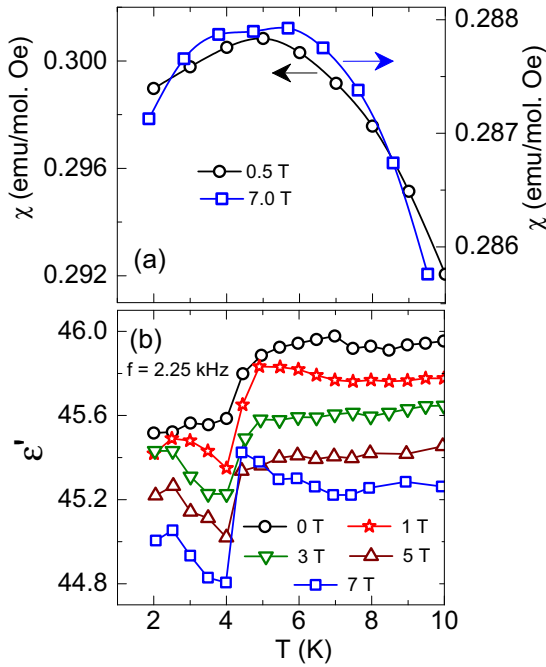


FIG. 7. (a) The dc magnetic susceptibility measured at 5 kOe and 7-T fields, indicating a cusp in the magnetization corresponding to a possible transition at 5 K. (b) Measurements of the dielectric constant in the same temperature range, as measured at different magnetic fields.

is not discernible in our specific-heat measurements, implying that the change in entropy associated with it is rather small, the transition is observed to be robust in the presence of large magnetic fields of the order of 7 T. Dielectric measurements [Fig. 7(b)] indicate a steplike feature at this temperature, reminiscent of that seen in many systems across their magnetic transitions. Measurements done at different magnetic fields show that there is no observable change in the nature of the magnetodielectricity on either side of this phase transition, suggesting that the nature of the polar state remains unchanged. This is also in agreement with our pyroelectric measurements which do not exhibit a peak in the pyrocurrent when the specimen is poled from a poling temperature of 15 K, thus ruling out the possibility of a new ferroelectric phase. Interestingly, on poling from temperatures above 35 K in the presence of large magnetic fields we observe that the polarization of the field-induced state remains well below 5 K. This clearly indicates that the field-induced ferroelectric state is not affected by this magnetic transition and also reinforces our observation that this low-temperature transition is not associated with a new polar state.

Our low-temperature M - H isotherms exhibit a nonsaturating behavior up to the highest applied field of 7 T, as expected for antiferromagnetic systems. A finite opening of the hysteresis loop is seen, possibly due to the presence of a finite ferromagnetic contribution, as was also indicated by the low value of the Curie-Weiss temperature θ_{CW} . Interestingly, we also observe the presence of a field-induced metamagnetic transition as evidenced by a change in slope in the M - H isotherms, which is seen more clearly in plots of dM/dT

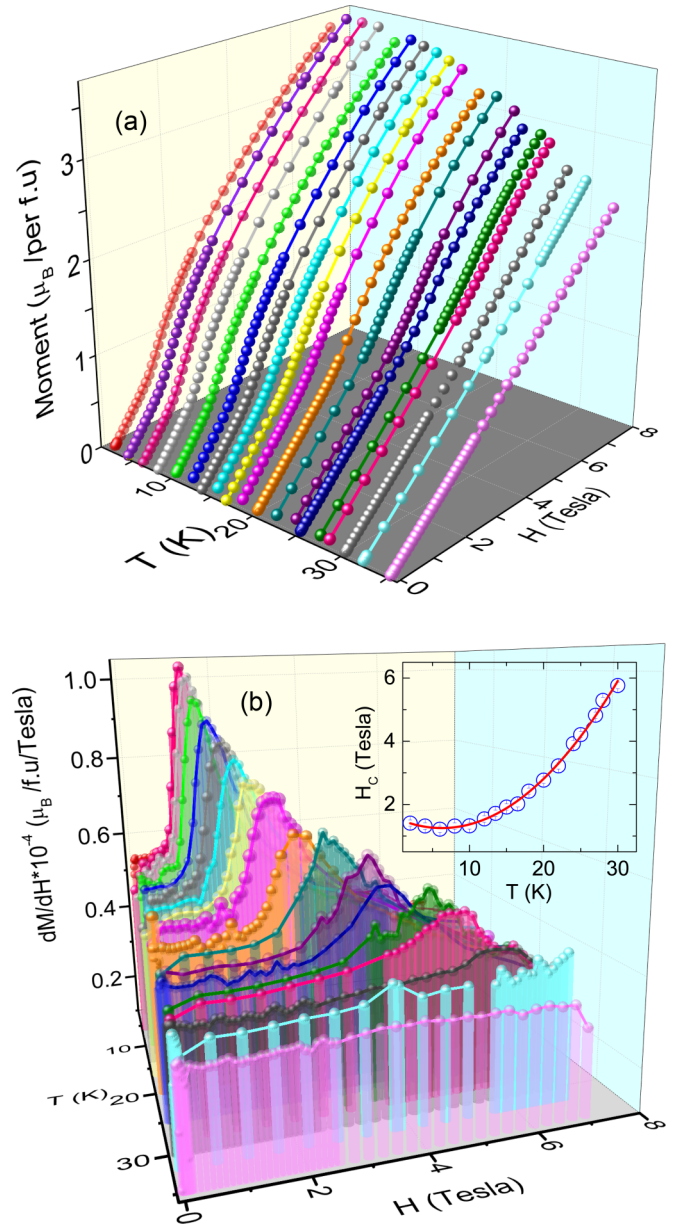


FIG. 8. (a) The low-temperature MH isotherms as measured at different temperatures. (b) The dM/dH of these isotherms to clearly identify the metamagnetic transition. The inset depicts the temperature evolution of the critical field H_C of the metamagnetic transition, with the solid line being a fit of the form $AT^2 + BT + C$.

vs T in the form of a peak (Fig. 8). The critical field associated with this metamagnetic transition is 1.4 T (± 0.1 T) at 2 K and steadily increases as a function of temperature. Interestingly, there is no apparent signature in the dielectric or pyroelectric measurements at the H - T values corresponding to this metamagnetic temperature, indicating that the polar state remains relatively unaltered. The critical field H_C associated with this transition has a slope $dH_C/dT > 0$ and also appears to have a T^2 dependence, as shown in the inset of Fig. 8. This is in broad agreement with Yamada's theory for itinerant metamagnets [24], which has been observed in a number of systems. However, it has to be borne in mind that this theory

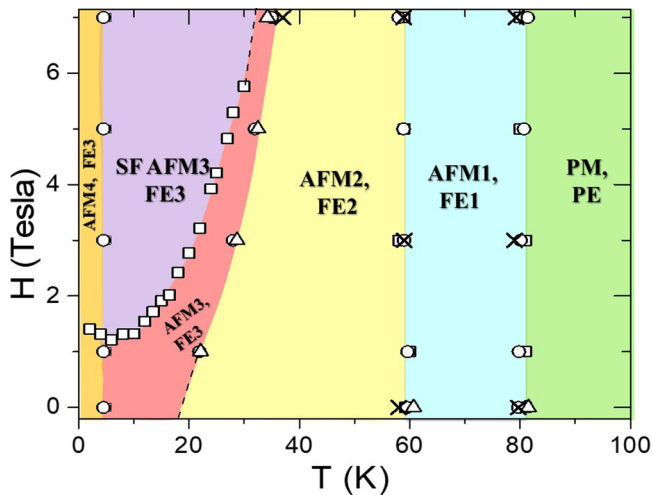


FIG. 9. The H - T phase diagram of $\text{Fe}_4\text{Ta}_2\text{O}_9$ as determined from magnetic (\square), specific-heat (\times), dielectric (\circ), and pyroelectric (\triangle) investigations. The dotted lines do not represent experimentally determined phase boundaries and are only meant as a guide to the eye.

was developed for field-induced paramagnetic-ferromagnetic phase transitions in itinerant magnets, and hence, its applicability within the antiferromagnetically ordered state of a system like $\text{Fe}_4\text{Ta}_2\text{O}_9$ is suspect.

The H - T phase diagram of $\text{Fe}_4\text{Ta}_2\text{O}_9$ as determined using the magnetic, thermodynamic, dielectric, and pyroelectric data at our disposal is depicted in Fig. 9. As a function of decreasing temperature, this system undergoes a transition into two distinct multiferroic states, labeled AFM1 FE1 and AFM2 FE2, at 80 and 60 K, respectively. On cooling further and in the presence of magnetic fields in excess of 1 T, we observe a field-induced multiferroic state denoted AFM3 FE3. Within this state, we also observe the presence of a metamagnetic (spin-flop) transition which appears to have no discernible influence on the polar state (SF-AFM3 FE3). At temperatures of the order of 5 K, we further observe the onset of possibly

a different kind of antiferromagnetic order (AFM4 FE3), as evidenced from magnetic and dielectric measurements. Needless to say, in-field neutron diffraction measurements would be imperative to reconfirm these phase boundaries and to identify the changes in the magnetic structure across these different phases. It is remarkable that $\text{Fe}_4\text{Ta}_2\text{O}_9$ exhibits such a complex phase diagram, which is in stark contrast to the other members of the extended $A_4\text{Ta}_2\text{O}_9$ family. We note that the phase diagram of this system has some parallels to that observed in the $\text{Ni}_3\text{V}_2\text{O}_8$ [25,26] and $\text{KCu}_3\text{As}_2\text{O}_7(\text{OD})_3$ [27] systems, stabilizing in distorted variants of the kagome structure, where a series of low-temperature magnetic phases coupled with polar order has been observed. A common factor here appears to be the presence of two-dimensional honeycomb layers which are buckled in and out of plane, with competing nearest- and next-nearest-neighbor interactions giving rise to a complex magnetic and polar phase diagram.

IV. CONCLUSIONS

In summary, using a combination of magnetic, thermodynamic, dielectric, and pyroelectric measurements, we demonstrated that $\text{Fe}_4\text{Ta}_2\text{O}_9$ is a multiferroic, in contrast to all the other members of its corundum-related family of materials. We speculate that this arises as a consequence of the inherently two-dimensional nature of the magnetically active sublattice that stabilizes in a buckled honeycomb structure. This system is also seen to exhibit a rich magnetic and polar phase diagram and could hence provide a useful playground for investigating the complex interplay between nearest and next-nearest magnetic interactions, anisotropy, and the Dzyaloshinskii-Moriya interactions in quasi-two-dimensional honeycomb lattices.

ACKNOWLEDGMENTS

The authors thank D. Buddhikot for his help with heat-capacity measurements. J.K. acknowledges DST India for support through Grant No. PDF/2016/0009/NPDF. S.N. acknowledges DST India for support through Grant No. SB/S2/CMP-048/2013.

-
- [1] M. Fiebig, T. Lottermoser, D. Meier, and M. Trassin, *Nat. Rev. Mater.* **1**, 1 (2016).
 [2] T. Kimura, *Annu. Rev. Mater. Res.* **37**, 387 (2007).
 [3] Y. Tokura and S. Seki, *Adv. Mater.* **22**, 1554 (2010).
 [4] S.-W. Cheong and M. Mostovoy, *Nat. Mater.* **6**, 13 (2007).
 [5] S. Park, Y. J. Choi, C. L. Zhang, and S.-W. Cheong, *Phys. Rev. Lett.* **98**, 057601 (2007).
 [6] I. Cabrera, M. Kenzelmann, G. Lawes, Y. Chen, W. C. Chen, R. Erwin, T. R. Gentile, J. B. Leão, J. W. Lynn, N. Rogado, R. J. Cava, and C. Broholm, *Phys. Rev. Lett.* **103**, 087201 (2009).
 [7] G. J. Nilsen, Y. Okamoto, H. Ishikawa, V. Simonet, C. V. Colin, A. Cano, L. C. Chapon, T. Hansen, H. Mutka, and Z. Hiroi, *Phys. Rev. B* **89**, 140412 (2014).
 [8] T. Kimura, J. C. Lashley, and A. P. Ramirez, *Phys. Rev. B* **73**, 220401 (2006).
 [9] I. E. Dzyaloshinskii, *J. Exp. Theor. Phys.* **10**, 628 (1959).
 [10] D. Astrov, *Sov. Phys. JETP* **11**, 708 (1960).
 [11] E. Bertaut, L. Corliss, F. Forrat, R. Aleonard, and R. Pauthenet, *J. Phys. Chem. Solids* **21**, 234 (1961).
 [12] I. V. Solov'yev and T. V. Kolodiazny, *Phys. Rev. B* **94**, 094427 (2016).
 [13] S. C. Abrahams, *Acta Cryst. B* **63**, 257 (2007).
 [14] E. Fischer, G. Gorodetsky, and R. Hornreich, *Solid State Commun.* **10**, 1127 (1972).
 [15] B. Liu, Y. Fang, Z. Han, S. Yan, W. Zhou, B. Qian, D. Wang, and Y. Du, *Mater. Lett.* **164**, 425 (2016).
 [16] Y. Fang, W. P. Zhou, S. M. Yan, R. Bai, Z. H. Qian, Q. Y. Xu, D. H. Wang, and Y. W. Du, *J. Appl. Phys.* **117**, 17B712 (2015).
 [17] Y. Fang, S. Yan, L. Zhang, Z. Han, B. Qian, D. Wang, and Y. Du, *J. Am. Ceram. Soc.* **98**, 2005 (2015).
 [18] N. D. Khanh, N. Abe, H. Sagayama, A. Nakao, T. Hanashima, R. Kiyonagi, Y. Tokunaga, and T. Arima, *Phys. Rev. B* **93**, 075117 (2016).

- [19] J. Rodriguez-Carvajal, *An Introduction to the Programme FULLPROF* (Laboratoire Leon Brillouin, CEA-CNRS, Saclay, France, 2001).
- [20] M. A. Castellanos R., S. Bernès, and M. Vega-González, *Acta Cryst. E* **62**, i117 (2006).
- [21] A. Scaramucci, E. Bousquet, M. Fechner, M. Mostovoy, and N. A. Spaldin, *Phys. Rev. Lett.* **109**, 197203 (2012).
- [22] B. Gallois, J. A. Real, C. Hauw, and J. Zarembowitch, *Inorg. Chem.* **29**, 1152 (1990).
- [23] S. F. Jin, Q. Huang, Z. P. Lin, Z. L. Li, X. Z. Wu, T. P. Ying, G. Wang, and X. L. Chen, *Phys. Rev. B* **91**, 094420 (2015).
- [24] H. Yamada, *Phys. Rev. B* **47**, 11211 (1993).
- [25] G. Lawes, A. B. Harris, T. Kimura, N. Rogado, R. J. Cava, A. Aharony, O. Entin-Wohlman, T. Yildirim, M. Kenzelmann, C. Broholm, and A. P. Ramirez, *Phys. Rev. Lett.* **95**, 087205 (2005).
- [26] N. R. Wilson, O. A. Petrenko, and G. Balakrishnan, *J. Phys.: Condens. Matter* **19**, 145257 (2007).
- [27] G. J. Nilsen, V. Simonet, C. V. Colin, R. Okuma, Y. Okamoto, M. Tokunaga, T. C. Hansen, D. D. Khalyavin, and Z. Hiroi, *Phys. Rev. B* **95**, 214415 (2017).